Demantoid from Kerman Province, South-east Iran: A Mineralogical and Gemmological Overview

Vahid Ahadnejad, Michael S. Krzemnicki and Ann Marie Hirt

ABSTRACT: Demantoid from Kerman Province in south-east Iran was investigated using microscopy, spectroscopy (optical absorption, FTIR and Raman), chemical analysis (EDXRF and LA-ICP-TOF-MS) and magnetic susceptibility measurements. The samples were transparent to semi-transparent and commonly contained acicular chrysotile inclusions. Their spectroscopic and chemical properties were consistent with demantoid from serpentinite host rock. The samples ranged from yellowish green to deep green, depending on Cr and Fe content. These two elements are also largely responsible for the material's paramagnetic susceptibility. Our samples contained relatively high concentrations of the trace elements Cr, Ge, Ni and Co. Comparison with available chemical data on serpentinite-hosted demantoid from the literature suggests that Iranian demantoid can be separated from stones of other localities.

The Journal of Gemmology, **38**(4), 2022, pp. 329–347, https://doi.org/10.15506/JoG.2022.38.4.329

Andradite, ideally $Ca_3Fe^{3+}_2Si_3O_{12}$, is the Ca-Fe end member of the ugrandite garnet subgroup and occurs in three colour-related varieties: black melanite, yellow to brown topazolite and yellowish green to green demantoid (Figure 1; O'Donoghue 2006). Demantoid usually contains traces of Cr, which is the main cause of the green colour, although stones from some deposits lack this element.

In 1853, Finnish mineralogist Nils Gustaf Nordenskiöld first described demantoid as a new variety of andradite from Nizhniy Tagil in the Central Ural Mountains of Russia (Eichmann 1870). Due to its exceptional brilliance and high dispersion, Nordenskiöld named the material *demantoid* ('diamond-like'). With a dispersion higher than that of diamond and its vivid green colour, it quickly became *au courant* at the Russian royal court as a treasured and expensive gem material.

For decades, demantoid was found almost exclusively in Russia (Phillips & Talantsev 1996). More recently, several other sources of gem-quality demantoid have been reported, such as Canada, Iran, Italy[1], Madagascar, Pakistan and Namibia (Lind *et al.* 1998; Quinn & Laurs

Figure 1: Demantoid from Iran is an attractive gem material. The stone shown here weighs 1.1 ct. Photo courtesy of K. Zebardast.

[1] Although demantoid from Val Malenco, Italy, was first described at the end of the 1800s, it only reached the market in recent decades.

Figure 2: This shaded relief map shows the location of the demantoid mining area near the village of Bagh Borj in Kerman Province (from Google Maps, https://tinyurl.com/2p8eu37y). The inset map indicates the location of this area (red rectangle) and Kerman Province (orange) in Iran.

2005; Du Toit *et al.* 2006; Karampelas *et al.* 2007; Adamo *et al.* 2009; Pezzotta *et al.* 2011). Most reports on demantoid have focused on its occurrence, crystal chemistry and gemmological properties (Gill 1978; Misiorowski & Hays 1993; Krzemnicki 1999; Milisenda *et al.* 2001; Pavese *et al.* 2001; Quinn & Laurs 2005; Adamo *et al.* 2015).

Gem-quality demantoid is commonly found in two very different geological settings (Adamo *et al.* 2011): serpentinite (e.g. Kerman Province, Iran; Val Malenco, Italy; Kaghan Valley, Pakistan; and Ural Mountains, Russia) and skarn (e.g. Antetezambato, Madagascar; and Erongo, Namibia). Most demantoid from serpentinite contains very fine and often curved needles, predominantly consisting of chrysotile, $Mg_3Si_2O_5(OH)_4$, a member of the kaolinite-serpentine group. These inclusions are characteristic of demantoid from Iran, Italy, Pakistan and Russia (Palke & Pardieu 2014). They do not, however, occur in skarn-related demantoid from Madagascar or Namibia. In addition, the chrysotile fibres in demantoid from serpentinites often radiate from a central chromite inclusion ($CrFe_2O_4$), forming what is commonly referred to as a 'horsetail' inclusion.

In this study, we focus on gem-quality demantoid from serpentinite-hosted deposits near the village of Bagh Borj (also called Bagh-e Borj) in the Soghan District of Kerman Province, south-eastern Iran.[2] Based on detailed fieldwork (by author VA) and laboratory analyses, we report on the geology, mineralogy and gemmology of this Iranian demantoid. In addition to collecting standard gemmological properties, we performed optical absorption spectroscopy, Fourier-transform infrared (FTIR) spectroscopy, Raman spectroscopy, chemical analyses and magnetic susceptibility measurements to characterise the samples.

LOCATION AND MINING

Iran's Kerman Province was first mentioned as a new source of gem-quality demantoid at the International Gemmological Conference in Spain in 2001 (Milisenda *et al.* 2001; Liu 2010). However, interviews by the first author (VA) with local villagers from Bagh Borj revealed that some Russian gem dealers were aware of this deposit many years earlier. These dealers occasionally bought demantoid of significant size and quality at rather low prices, so it is possible that some of the material marketed as being of Russian origin might have actually come from Iran.

The demantoid mining area is located between the towns of Jiroft and Baft in Kerman Province, about 960 km south-east of Tehran (Figure 2). High-quality demantoid

[2] Not included in this study is skarn-related demantoid from deposits in western and north-western Iran (Takab, Sarab, Hormozgan and Kurdistan). Although these localities have occasionally produced large crystals, they are usually highly fractured and thus of only limited use as gems.

Figure 3: (**a**, **b**) Demantoid mining near Bagh Borj has been done in tunnels and open cuts excavated by local residents. The underground workings can reach more than 50 m. (**c**) Demantoid is hosted by weathered serpentinite and is easily separated from it. (**d**) These demantoid crystals average 1 g each. Photos by V. Ahadnejad.

was first found near Bagh Borj, which is located in a cold, mountainous region. The roads to the village are very rugged and cannot be passed by car during the winter season. Additional garnet localities have been mined by local inhabitants of other villages in this region, such as Solouiyeh, Rosedar, Madan-e Abdasht, Sargaz, Parantabad, Anbarabad, Fathabad, Dowlatabad and Vakilabad. However, gem-quality demantoid has not yet been found at most of these locations; almost all commercially significant production has been mined in the mountains around Bagh Borj (Figure 3).

Currently, the annual production of demantoid from the Bagh Borj area is estimated at several thousand grams of rough material of various qualities. The weight of a piece of rough seldom exceeds 0.2 g (Figure 4), but occasionally larger crystals are produced (up to 1 g) and, very rarely, even some giant ones weighing up to several dozen grams (Figure 5). However, most of the larger crystals are quite included. The gem-quality material is consumed by the jewellery trade in Iran and also exported to Europe, India and China, both as rough and cut stones.

Figure 4: These small crystals (approximately 0.2 g each) of gem-quality Iranian demantoid show attractive vivid green to yellowish green colour and excellent transparency. Photo courtesy of A. Badamegan.

Figure 5: This giant demantoid crystal from Kerman Province weighs 137 g. Photo by V. Ahadnejad.

GEOLOGICAL SETTING

The demantoid deposits in Kerman Province are located in the south-eastern part of the Sanandaj-Sirjan zone, an elongated geological system (about 1,500 km long and 70 km wide) extending north-west to south-east throughout Iran (Figure 6). It represents the north-eastern suture of the Neo-Tethys that formed by continental collision between the northern margin of Gondwana and the southern part of Eurasia during the late Eocene (Allen & Armstrong 2008) or Oligocene (McQuarrie & van Hinsbergen 2013). The Sanandaj-Sirjan zone contains scattered elements of Pan-African basement rocks, interpreted as the south-western margin of the Cimmerian continental fragment (Celâl Şengör 1984; Ricou 1994; Stampfli & Borel 2002; Fergusson *et al.* 2016). The continental collision was preceded by complex tectonic events that followed Mesozoic convergence along the Tethys Ocean's northern margin and ophiolite obduction on its southern margin.

The Sanandaj-Sirjan zone consists of highly deformed metamorphic rocks, including ophiolitic mélange (ophiolitic blocks mixed with serpentinite and pelagic sediments and flysch) and ultramafic-mafic complexes that indicate an active tectonic regime (Ahmadipour *et al.* 2003; Barrois *et al.* 2012, 2013). Ophiolites represent former oceanic crust and underlying mantle materials that have been tectonically uplifted to the surface, typically during the closing of an ocean basin. They consist of an assemblage of mafic and ultramafic lavas and hypabyssal rocks found in association with sedimentary rocks, such as greywacke and chert. Most of the ultramafic rocks are altered to serpentinite.

Investigations by author VA showed that the green fibrous serpentinite that hosts most of the demantoid occurrences in Kerman Province is very soft (like soapstone) and consists of chrysotile, antigorite, bastite (as a pseudomorph), brucite and talc. Chromite, which is potentially the source of Fe and Cr in the demantoid, is abundant in the serpentinised rocks. Several chromite deposits are exploited in the area, such as the Abdasht mine with an ore concentration of 35–40% Cr_2O_3. There is a close relationship between Cr deposits and demantoid genesis. The study area (Bagh Borj and its surroundings) consists of oceanic lithosphere that is represented by ophiolitic sequences including peridotites. These peridotites were uplifted along detachment faults and underwent hydrothermal alteration. The mineral association—including chromite, magnesiochromite, Cr-spinel, picotite, uvarovite and magnetite—imply

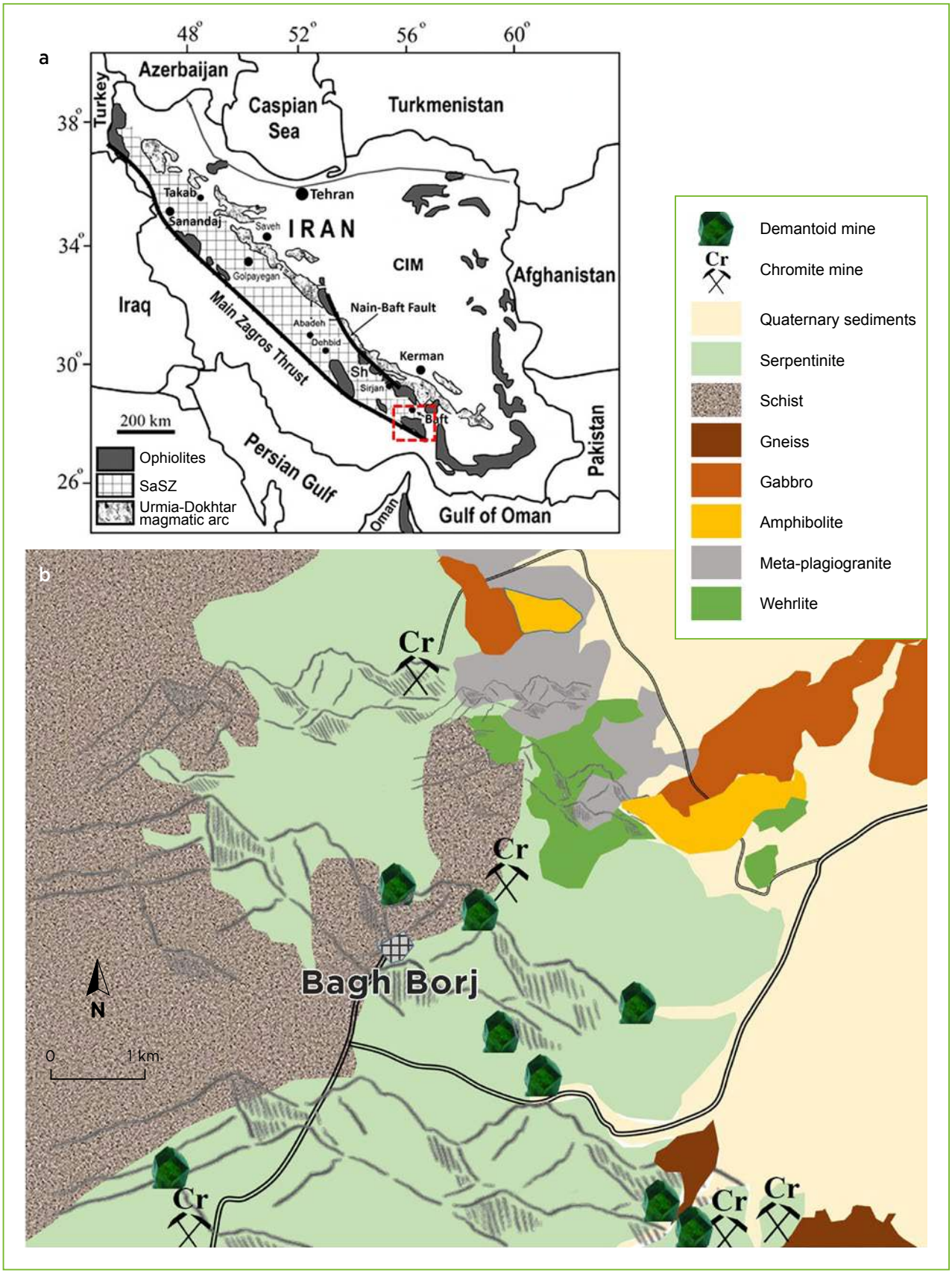

Figure 6: (**a**) Demantoid deposits in Iran's Kerman Province are hosted by ophiolitic rocks at the south-east end of the Sanandaj-Sirjan Zone (SaSZ; see red rectangle; modified after Emami *et al.* 1993 and Ghazi *et al.* 2011). (**b**) The local geological map of Bagh Borj (after Shahraki-Ghadimi *et al.* 2002) shows the distribution of the main rock types, including serpentinite, which hosts the demantoid localities as well as chromite deposits in the area.

a hydrothermal system containing Cr and Fe associated with demantoid genesis in the fissures and veins within metasomatised serpentinite. Finally, the tectonically convergent movements of Iranian-Arabian plates caused uplift of the crust and exposure of demantoid-bearing serpentinite. Demantoid is loosely bound by the serpentinite matrix and therefore crystals may appear in the local rivers after heavy rain.

MATERIALS AND METHODS

From a large parcel of rough demantoid, partly collected by one of the authors (VA) and partly bought from local miners in the Bagh Borj area, we selected 10 representative gem-quality rough samples originating from various localities within the study area (Table I). A window was cut and polished on one side of each specimen to facilitate analyses and observation of internal features. These samples (0.25–1.02 g) ranged from yellowish green to vivid green and were transparent to semi-transparent. In addition, two faceted demantoid gemstones (0.63 and 0.80 ct) from Kerman Province were used for standard gemmological testing and microscopic examination.

All the specimens were analysed at the Swiss Gemmological Institute SSEF in Basel, Switzerland, with standard gemmological tools including a refractometer, a hydrostatic balance, long- and short-wave UV lamps, and a microscope. Optical absorption spectra (375–900 nm) were collected using a Cary 500 spectrophotometer with a scan rate of 70 nm/minute and a data interval of 0.35 nm. FTIR spectra were recorded with a Thermo Nicolet iS50 spectrometer using the condensed beam mode and 4.0 cm^{-1} resolution. Each analysis consisted of 256 scans of the sample and background. Raman spectroscopy of demantoid and the inclusions in selected samples was performed with a Renishaw inVia confocal Raman microscope equipped with an argon-ion laser (514.5 nm), using 20× magnification and a resolution of about 1.5 cm^{-1}.

The chemical composition of each sample was measured at SSEF by energy-dispersive X-ray fluorescence (EDXRF) spectroscopy using a Thermo Scientific ARL Quant'X instrument. All specimens were analysed under vacuum with five different excitation energies (8, 12, 16, 25 and 40 kV) to optimise sensitivity for silicate analysis. In addition, each of the samples was analysed at SSEF with laser ablation inductively coupled plasma time-of-flight mass spectrometry (LA-ICP-TOF-MS, referred to below as GemTOF). The instrument consisted of a high-performance 193 nm laser ablation unit (NWR193UC from ESI, Huntingdon, UK) coupled to an ICP-TOF-MS (icpTOF from Tofwerk AG, Thun, Switzerland). Detailed information about instrumental parameters, analytical conditions and raw data processing can be found in Wang *et al.* (2016), Phyo *et al.* (2020) and Wang & Krzemnicki (2021). The benefit of TOF-MS (compared with more conventional quadrupole MS) is the simultaneous acquisition of the full mass spectrum, which makes it ideal for constantly monitoring elemental

Table I: Demantoid study samples and their localities in Kerman Province, Iran.

Sample no.	Main colour	Weight (g)	Latitude	Longitude	Nearest town (village)	Lithology
1	Green	1.02	28° 44′ 27.7″	57° 28′ 16.0″	Jiroft (Sargaz)	Serpentinised lherzolite
2	Dark green	0.83	28° 33′ 21.4″	57° 09′ 32.5″	Jiroft (Bagh Borj)	Serpentinised lherzolite
3	Light green	0.59	28° 29′ 37.5″	56° 53′ 37.4″	Baft (Parantabad)	Serpentinite schist
4	Yellowish green	0.57	28° 24′ 05.3″	56° 56′ 43.1″	Baft (Anbarabad)	Serpentinite schist
5	Green	0.53	28° 20′ 21.2″	56° 45′ 23.7″	Baft (Madan-e-Abdasht)	Serpentinised lherzolite
6	Dark green	0.37	28° 15′ 43.6″	56° 46′ 35.6″	Baft (Fathabad)	Serpentinised dunite
7	Green	0.32	28° 15′ 05.3″	56° 45′ 01.8″	Baft (Fathabad)	Serpentinite schist
8	Olive green	0.39	28° 12′ 59.9″	56° 25′ 56.4″	Baft (Dowlatabad)	Serpentinite schist
9	Yellowish green	0.36	28° 18′ 59.0″	56° 22′ 51.4″	Orzueeyeh	Serpentinised dunite
10	Dark green	0.25	28° 22′ 36.9″	56° 05′ 09.5″	Orzueeyeh (Vakilabad)	Serpentinised lherzolite

variations (such as those due to growth zoning), and also detecting accidentally ablated (sub-microscopic) inclusions (Wang *et al*. 2016). We analysed three spots with an ablation diameter of 100 µm on visually inclusion-free areas of each sample. NIST SRM 612 glass was used as the external standard and stoichiometric Si (for ideal andradite) as the internal standard.

Some demantoids are attracted by a strong magnet due to their relatively high Fe content. To investigate this, we tested 84 demantoid crystals from the study area with a very strong neodymium magnet that measured 2 × 10 × 20 mm. In addition, we measured the magnetic susceptibility (see Box A) of the 10 demantoid samples characterised for this report in order to collect data that might be useful in the future for separating Iranian demantoid from its counterparts from other localities. Magnetic susceptibility can indicate if ferromagnetic inclusions are present and may also provide information regarding chemical variability. The magnetic susceptibility and its directional dependence—that is, the anisotropy of magnetic susceptibility (AMS)—was analysed at ETH Zurich in Switzerland with an AGICO MFK1-FA Kappabridge instrument, using an applied field of 200 A/m and a frequency of 976 Hz. AMS is mathematically described by a symmetric second-order tensor, and can be geometrically represented with an ellipsoid whose principal axes are the three eigenvalues of the tensor, where $K_1 \geq K_2 \geq K_3$. Mean magnetic susceptibility (K_m) is defined as:

$$K_m = (K_1 + K_2 + K_3)/3$$

Induced magnetisation as a function of high field was used to determine if there were any ferromagnetic inclusions present. Because the bulk susceptibility turned out to be similar for all samples, only one of them was evaluated in this way. Garnet is a paramagnetic mineral and should follow the Curie law, in which $K = C/(T-\theta_p)$, where C is a constant, T is temperature and θ_p is the paramagnetic Curie temperature. The value of θ_p has not been experimentally determined, but is an important and unique magnetic property of a mineral. The induced magnetisation was measured on a Princeton Measurements Corporation vibrating sample magnetometer outfitted with a liquid helium cryostat in fields of ±1 tesla and temperatures between 20 and 270 K.

BOX A: MAGNETIC SUSCEPTIBILITY

The characterisation of the magnetic properties of materials is a rather rarely applied method for gem identification and classification, although it has been used for determining the purity of diamond for a number of decades (Sigamony 1944). In general, materials can be separated into three categories based on their reaction to a magnetic field:

1. *Diamagnetic* materials have no magnetic moment when no magnetic field is applied and a negative susceptibility when a magnetic field is applied (i.e. the induced magnetic moment is in the opposite direction from the applied field).
2. *Paramagnetic* materials also have no magnetic moment when no magnetic field is applied, but have a weak magnetic moment in the direction of the applied magnetising field, and therefore have a positive magnetic susceptibility.
3. *Ferromagnetic* materials retain their magnetisation in the absence of an applied field over time. Their susceptibility is positive and can be significantly stronger than that of paramagnetic materials.

Because magnetic susceptibility is directly dependent on the elemental composition of a mineral (particularly Fe content), it can be useful in the study of gems. Hoover (2011) demonstrated that by combining information on RI and magnetic susceptibility, the chemical composition of garnets can be inferred. In the case of olivine, a quantitative relationship between magnetic susceptibility and Fe content has been used to determine the fayalite mole fraction (cf. Hoye & O'Reilly 1972). Pure forsterite is diamagnetic (due to the absence of Fe) and has a mass susceptibility of about -3.9×10^{-9} m^3/kg. Olivine may become paramagnetic due to the presence of Fe, whereby the mass susceptibility increases with greater Fe content, reaching a value of 1.1×10^{-6} m^3/kg for pure fayalite. Typical peridot gains its green colour from Fe and has a much higher magnetic susceptibility index (~500) than colourless forsterite (~52; Feral 2010).

Furthermore, the maximum susceptibility in peridot is parallel to the *c*-axis (Biedermann *et al*. 2014). The anisotropy of magnetic susceptibility can be used to determine the orientation of the *c*-axis and thus can help the lapidary obtain the best colour of a cut stone.

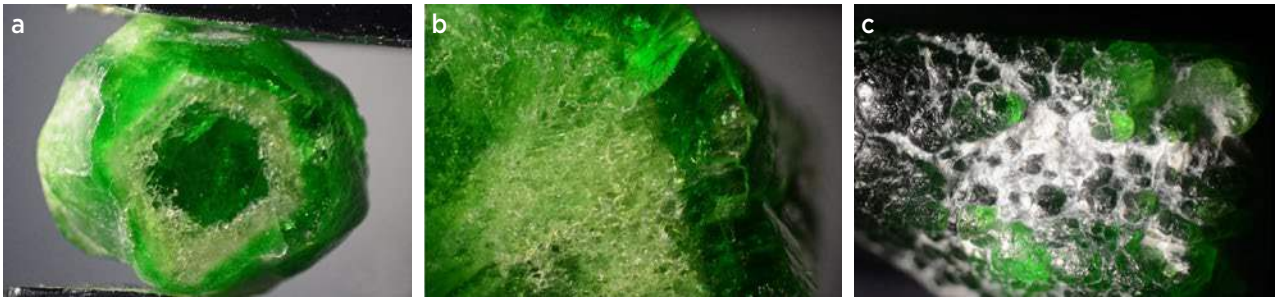

Figure 7: (**a**) Distinct colour zoning in demantoid sample no. 5 shows a rather transparent green core surrounded by a yellowish green intermediate zone containing a dense micro-crack pattern and followed by a vivid green rim. (**b**) A closer view of the intermediate zone shows the honeycomb-like pattern of the micro-cracks. (**c**) The botryoidal surface of serpentinite-related demantoid is seen on this specimen. Photos by M. S. Krzemnicki; magnified (a) 10×, (b) 50× and (c) 30×.

RESULTS

Standard Gemmological Testing

Testing of our samples by classical gemmological methods gave results consistent with the reported physical properties for demantoid (cf. O'Donoghue 2006). The SG value ranged from 3.82 to 3.87. The RI could not be measured using a standard refractometer (based on total internal reflection) because the value is above that of the contact liquid (i.e. >1.81). Under long-wave UV radiation, our samples were inert or showed very weak yellowish green fluorescence, and they were inert to short-wave UV.

Microscopic Observations

The investigated demantoid samples were quite included. Most exhibited distinct angular growth zones with a saturated green core surrounded by a yellowish green intermediate zone that was overgrown by a vivid green rim (Figure 7a). The intermediate zone locally exhibited a dense pattern of honeycombed micro-cracks, whereas the rim of the crystals was commonly characterised by a botryoidal outline and tiny radial fissures (Figure 7b, c). Similar botryoidal surfaces are well known in serpentinite-related demantoid from other deposits. The faceted stones examined for this study displayed both colour zoning and micro-cracks, which were common in the culet area (Figure 8a–c).

Straight-to-curved fibres were the most prominent inclusion feature. They usually were present mostly in the rim zone as fine bundles or layers of rather parallel fibres (partly chrysotile, partly hollow; Figure 8d–f) or in the core of the crystals as randomly oriented curved fibres (Figure 8d). Raman micro-spectroscopy of several whitish fibrous inclusions in one sample revealed that

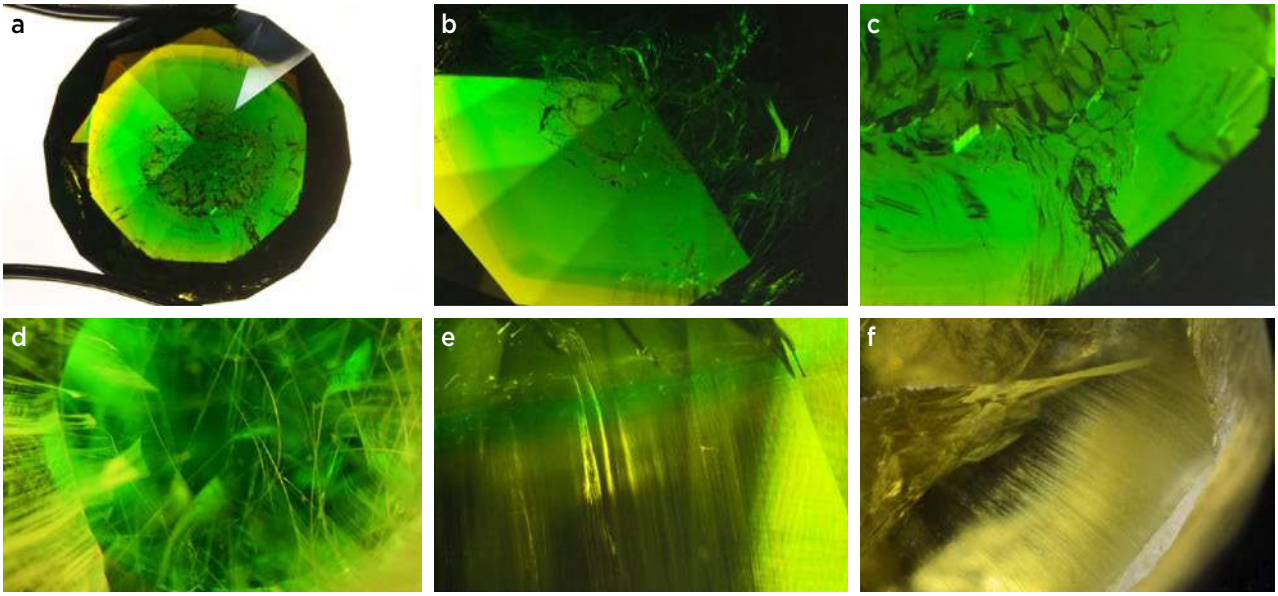

Figure 8: A faceted demantoid from Kerman Province reveals colour zoning (**a**, **b**), micro-cracks in the culet area (**a**–**c**) and fine fibres (**d**–**f**). These fibres occur in bundles or layers in the intermediate and rim zones, but most of the fibres in the core are distinctly curved. Photomicrographs by M. S. Krzemnicki; magnified (a) 10×, (b) 20×, (c) 30×, (d, e) 40× and (f) 50×.

they consisted of chrysotile (see Raman section below). Fibrous calcite, as reported by Karampelas *et al.* (2007), was not found in our samples.

In some cases, the fibres were aggregated into small whitish 'cotton balls'. Although small black chromite inclusions were present, our samples showed no radiating 'horsetails' from these grains, as known in demantoid from serpentinite-related deposits such as in Russia and Val Malenco, Italy (Laurs 2002; Du Toit *et al.* 2006; Karampelas *et al.* 2007; Adamo *et al.* 2009; Liu 2010; Hennebois *et al.* 2021). In addition, most samples contained fine veils of partially healed fissures ('fingerprints').

As reported in the gemmological literature, Iranian demantoid occasionally exhibits a cat's-eye effect when properly cut as a cabochon. This effect is caused by long parallel fibrous inclusions (Laurs 2002; Douman & Dirlam 2004; Kiefert & Koivula 2005; Karampelas *et al.* 2007; Liu 2010). However, we did not see any chatoyancy in our samples.

Optical Absorption Spectroscopy

To better understand the colour variations seen in Iranian demantoid, we analysed five samples: green (no. 1), light green (no. 3), olive green (no. 8), yellowish green (no. 9) and dark green (no. 10), thus covering the full range of colours we observed in demantoid from Kerman Province. The spectra of all samples were dominated by Cr^{3+} absorption bands at 625 and 640 nm (Figure 9), consistent with demantoid from other serpentinite-hosted deposits (e.g. Russia and Val Malenco, Italy). Samples 3 and 8 also showed an Fe^{3+}-related peak at around 440 nm, but this feature could not be observed in the others due to their absorption edges. A more detailed analysis of those spectra revealed that overlapping absorption of Cr^{3+} and Fe^{3+} chromophores leads to the absorption edge at around 390 nm.

The 440 nm Fe^{3+} band was narrow and displayed a sharp edge. A shoulder at about 465 nm, most visible for the green sample (no. 1), is presumably due to a broad chromium band towards the UV. It was not present in the Cr-poor yellowish green sample (no. 9). Samples 3 and 8 also showed a transmission window at about 400 nm.

Thus, common features among our samples include: (a) very strong Fe^{3+} absorption between 430 and 444 nm; (b) a shoulder between approximately 465 and 480 nm; (c) a weak band at around 690 nm that is correlated

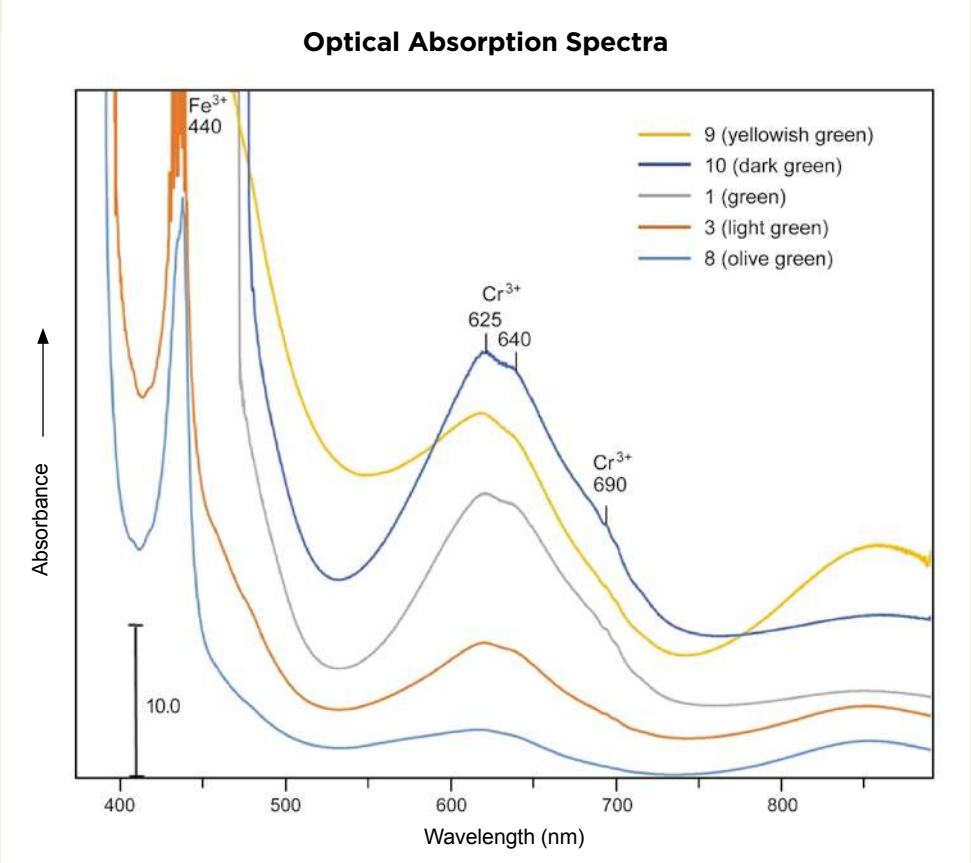

Figure 9: The optical absorption spectra of the demantoid samples are characterised by a broad absorption band caused by peaks at 625 and 640 nm related to Cr^{3+}. Samples 3 and 8 also show a distinct Fe^{3+} peak at about 440 nm. The absorption edge in the blue region of the spectrum is due to overlapping features related to Cr^{3+} and Fe^{3+}. The spectra are offset vertically for clarity. The path lengths of the beam were 3.0 mm (no. 1), 3.8 mm (no. 3), 4.2 mm (no. 8), 5.2 mm (no. 9) and 3.7 mm (no. 10).

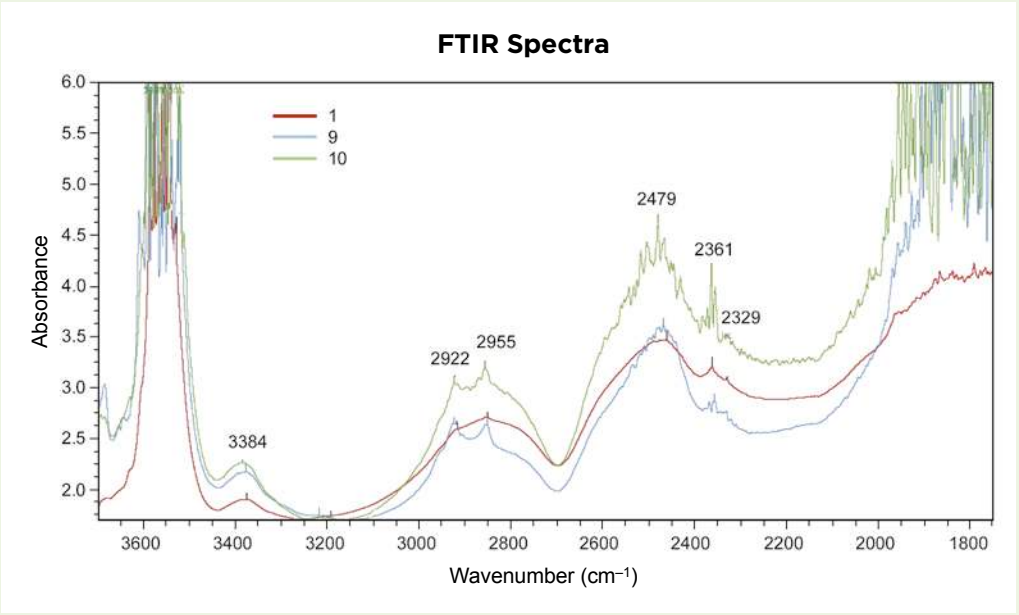

Figure 10: FTIR spectra for selected demantoid samples (nos. 1, 9 and 10) show a large asymmetric band at about 3500 cm^{-1} related to the presence of OH^-.

to Cr^{3+}; (d) strong Cr^{3+} absorption bands at 625 and 640 nm; and (e) a main transmission window between 530 and 535 nm that accounts for the green colour of demantoid. The samples show different absorption levels that correspond to their variations in colour.

FTIR Spectroscopy

The FTIR spectra in the 3700–1800 cm^{-1} region of three demantoid samples (nos. 1, 9 and 10) are shown in Figure 10. The large asymmetric band at about 3500 cm^{-1} is related to the presence of OH^- (Amthauer & Rossman 1998; Adamo *et al.* 2011; Geiger & Rossman 2018).

The FTIR spectra show a good match with those of typical andradite.

Raman Spectroscopy

The Raman spectra of the samples are also characteristic for andradite, with main peaks at 371 and 515 cm^{-1}, and a triplet at 817–875 cm^{-1} (Figure 11). Also present are a H_2O-related peak at 3703 cm^{-1}, and photoluminescence

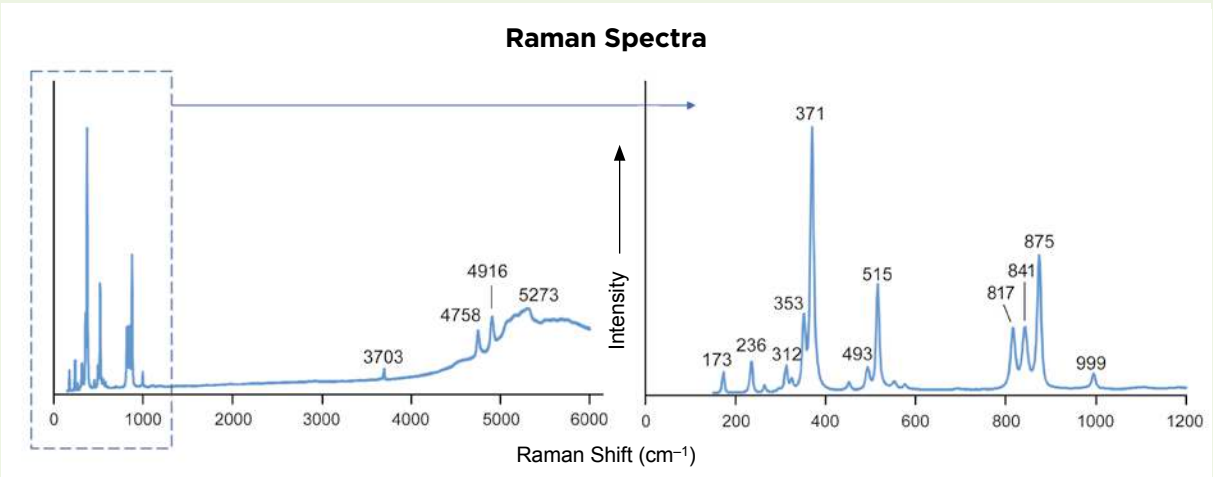

Figure 11: Raman spectra for a representative demantoid sample (no. 7) show main peaks at 371 and 515 cm^{-1}, as well as a triplet at 817–875 cm^{-1}, an H_2O-related peak at 3703 cm^{-1} and photoluminescence peaks at 4750–5300 cm^{-1} that are presumably related to Cr^{3+}.

peaks at 4750–5300 cm^{-1} presumably related to Cr^{3+} (681.3 and 688.7 nm and a multiband series centred at 706.1 nm; Gaft *et al.* 2005; Jasinevicius 2009).

Raman spectroscopy of a whitish fibrous inclusion in sample 2 provided the best fit with that of chrysotile in the RRUFF database (https://rruff.info), showing main Raman bands at 1103, 690, 620, 387 and 233 cm^{-1} (Rinaudo *et al.* 2003; Petriglieri *et al.* 2015).

Chemical Analysis

EDXRF chemical data for the demantoid samples are presented in Table II. Although the ten specimens came from three different locations in the Bagh Borj area (see Table I), their compositions were very similar. As expected for andradite, the samples contained elevated Fe (mean value of 32.21 wt.% Fe_2O_3) and Ca (36.05 wt.% CaO), but also a considerable amount of Cr (2.31 wt.% Cr_2O_3). Also present were minor amounts of Mg (1.20 wt.% MgO) and traces of Mn (0.17 wt.% MnO), K (0.10 wt.% K_2O) and V (0.02 wt.% V_2O_3). Thus, the analysed specimens had only small pyrope and very small spessartine components. Sample 9 (slightly yellowish green) contained distinctly lower Cr than those showing a more vivid green colour.

Chemical data obtained with the GemTOF instrument are presented in Table III. As noted for the EDXRF analyses, Fe was the predominant transition metal in the samples, followed by Cr, Mn, Ti and V (Table III). Additional trace elements included Co, Ni, Ge>Ga, As, Sr, Y, Zr, Nb, Sn, Hf, Ta, REE, W and U>Th.

Magnetic Susceptibility

Testing of 84 Iranian demantoid crystals with a very strong neodymium magnet showed that 72 of them (85%) had weak to strong attraction to the magnet, while only 12 crystals were inert.

The mean mass magnetic susceptibility of the 10 analysed demantoid samples was between 6.00×10^{-7} to 6.54×10^{-7} m^3/kg, with an average value of 6.38×10^{-7} m^3/kg (Table II). The magnetic susceptibility of all samples was isotropic (i.e. it was not dependent on the direction of the applied field).

The specimen that was evaluated as a function of high field at temperatures between 20 and 270 K showed an induced magnetisation that was linearly related to the applied field for all temperatures (Figure 12a), which indicates that the sample is paramagnetic in this temperature range and that no ferromagnetic inclusions are present. The increase in magnetic susceptibility with decreasing temperature follows the Curie Law, as seen from the linear trend of inverse susceptibility as a function of temperature (Figure 12b). Because the projection of the linear trend extends to a temperature of <0 K, the projected value of the paramagnetic Curie temperature

Table II: Chemical composition by EDXRF and magnetic susceptibility of demantoid from Kerman Province, Iran.

Oxide (wt. %)	1	2	3	4	5	6	7	8	9	10
SiO_2	29.22	27.37	29.68	28.26	29.03	26.45	26.78	26.27	25.99	27.28
Al_2O_3	bdl*	bdl	bdl	bdl	bdl	bdl	bdl	bdl	bdl	bdl
Cr_2O_3	1.77	2.73	1.46	2.32	2.04	2.77	2.93	2.70	0.33	4.09
V_2O_3	0.015	0.004	0.011	0.013	0.026	0.032	0.026	0.024	0.021	0.031
Fe_2O_3	33.48	31.05	34.03	33.63	33.42	31.41	30.69	30.88	35.31	28.23
MnO	0.14	0.18	0.11	0.16	0.17	0.17	0.21	0.19	0.10	0.21
MgO	0.88	0.30	0.53	0.66	1.01	0.60	2.47	2.07	0.43	3.06
CaO	34.18	37.99	33.81	34.61	33.95	38.16	36.46	37.43	37.39	36.56
K_2O	0.07	0.08	0.08	0.10	0.10	0.10	0.11	0.11	0.14	0.12
Total	99.76	99.70	99.71	99.75	99.75	99.69	99.68	99.67	99.71	99.58
Magnetic susceptibility (10^{-7} m^3/kg)	6.11	6.00	6.42	6.54	6.46	6.49	6.37	6.48	6.51	6.47

* Al_2O_3 was below the detection limit (bdl) of our EDXRF setup in all analyses. In addition, S, Ga, Ge, As, Rb, Sr, Zr, Sb, Cs, Ba and Pb were not detected.

Table III: Chemical analyses by GemTOF of demantoid from Kerman Province, Iran.*

Element (ppmw)	1	2	3	4	5	6	7	8	9	10
Sc	48.5	62.6	16.6	115.1	2092	137.4	80.8	95.2	36.1	78.7
Ti	126.2	419.0	34.2	202.6	62.0	133.4	237.3	241.5	109.8	238.2
V	136.1	174.3	21.8	77.7	25.2	196.2	102.4	75.0	99.1	61.7
Cr	26830	31720	1117	18390	11060	18590	29080	22170	4032	26720
Mn	235	242	245	267	256	226	255	250	297	260
Al	68.78	38.64	143.2	102.3	123.8	45.86	67.26	79.04	284.7	98.96
Fe	213280	210890	238100	216090	224560	220160	212880	216870	236340	211140
Co	3.05	2.77	3.55	3.46	2.95	2.33	2.86	2.83	2.17	2.72
Ni	na	3.80	6.32	9.22	3.69	4.47	9.81	na	2.82	5.46
Cu	0.401	0.225	0.275	0.174	0.240	0.457	0.222	0.400	0.219	0.256
Ga	0.127	0.156	0.084	0.065	0.097	0.137	0.132	0.102	0.138	0.095
Ge	27.5	32.2	22.5	25.8	22.5	35.5	26.8	27.4	25.2	22.4
As	0.529	0.496	0.520	0.451	0.542	0.410	0.369	0.452	0.410	0.356
Sr	0.377	0.219	0.496	0.235	0.295	0.277	0.190	0.202	0.106	0.293
Y	0.726	0.775	0.058	1.678	0.123	2.50	1.05	1.24	0.284	0.617
Zr	1.38	2.27	0.069	1.18	0.107	2.87	1.71	1.91	0.896	0.799
Nb	0.745	8.70	na	0.430	0.048	0.232	0.323	0.503	0.248	0.541
Sn	2.37	2.47	1.26	1.41	1.73	1.89	1.41	0.97	3.23	1.19
Hf	0.054	0.067	0.007	0.053	0.008	0.093	0.056	0.048	0.022	0.027
Ta	0.011	0.170	0.003	0.007	na	0.003	0.005	0.006	na	0.007
W	1.82	0.049	3.24	3.43	4.37	1.83	1.79	2.82	na	3.71
Th	0.008	0.015	0.010	0.040	0.018	na	0.026	0.065	0.013	0.061
U	0.047	0.056	0.086	0.123	0.125	0.023	0.106	0.160	0.400	0.131
La	0.062	0.052	0.133	0.128	0.140	0.045	0.097	0.162	0.197	0.147
Ce	0.282	0.392	0.288	0.596	0.346	0.190	0.488	0.908	0.548	0.701
Pr	0.049	0.081	0.018	0.072	0.024	0.039	0.072	0.098	0.022	0.081
Nd	0.287	0.307	0.053	0.254	0.054	0.200	0.255	0.336	0.055	0.224
Sm	0.082	0.046	na	0.104	0.048	0.052	0.045	0.051	na	0.104
Eu	0.011	0.017	na	0.021	0.009	0.028	0.015	0.018	0.013	0.016
Gd	0.038	0.045	na	0.111	na	0.096	0.049	0.060	0.030	0.046
Tb	0.008	0.009	0.004	0.021	0.005	0.024	0.013	0.010	0.007	0.010
Dy	0.083	0.068	0.014	0.201	0.017	0.275	0.128	0.094	0.037	0.076
Ho	0.025	0.025	0.003	0.077	0.005	0.092	0.029	0.036	0.009	0.018
Er	0.114	0.111	0.009	0.287	0.020	0.411	0.176	0.194	0.038	0.094
Tm	0.311	0.027	na	0.069	0.004	0.072	0.059	0.045	0.008	0.023
Yb	0.272	0.311	0.022	0.750	0.029	0.649	0.508	0.587	0.067	0.317
Lu	0.067	0.079	0.002	0.175	0.007	0.131	0.131	0.155	0.014	0.083
Σ REE	1.69	1.57	0.55	2.87	0.71	2.30	2.07	2.75	1.05	1.94
Σ LREE	0.77	0.90	0.49	1.18	0.62	0.55	0.97	1.77	0.84	1.27
Σ HREE	0.92	0.68	0.05	1.69	0.09	1.75	1.09	1.18	0.21	0.67
Σ LREE / Σ HREE	0.84	1.33	9.11	0.69	7.14	0.32	0.89	1.33	3.98	1.91

* Mean values of three analyses each. Abbreviation: na = not analysed.

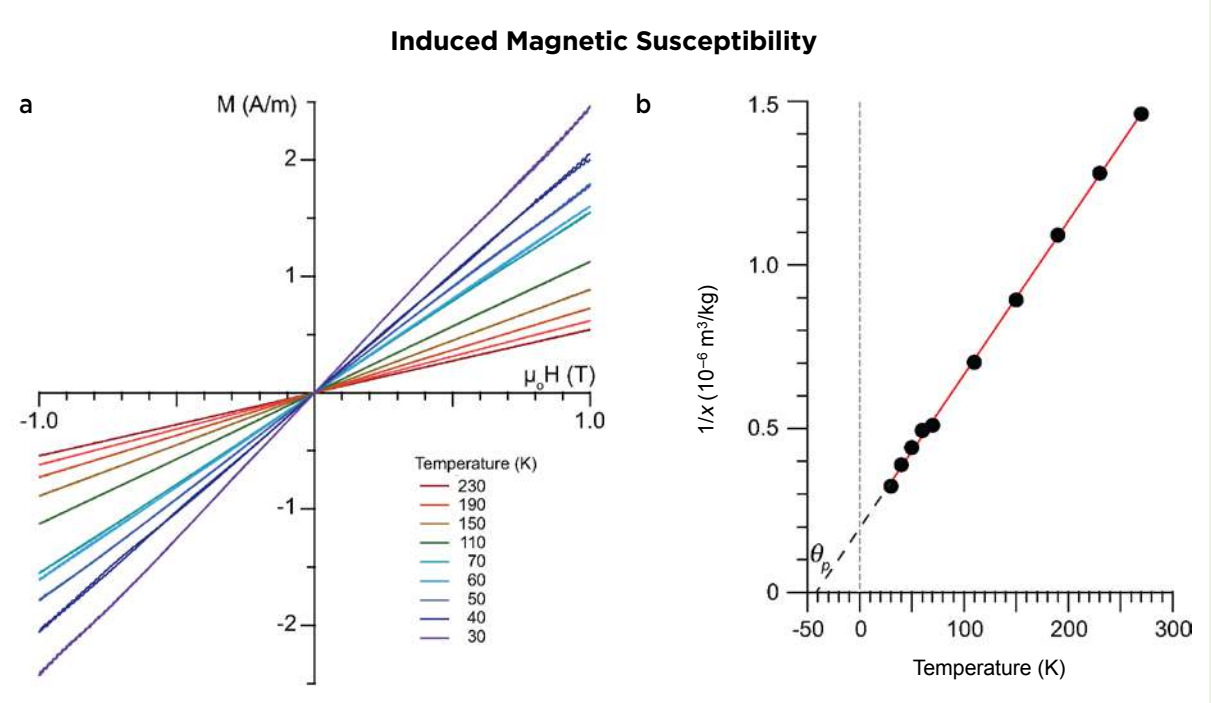

Figure 12: (**a**) For a representative demantoid sample, induced magnetisation as a function of applied field at different temperatures illustrates its paramagnetic behaviour. (**b**) Inverse susceptibility as a function of temperature shows a linear temperature dependency and a projected value of the paramagnetic Curie temperature θ_p = –41.9 K.

is negative with θ_p = –41.9 K. In this case, θ_p is referred to as the asymptotic Néel temperature[3] because the demantoid must undergo antiferromagnetic ordering at a very low temperature (Néel 1948). The asymptotic Néel temperature is indicative of a predominantly antiferromagnetic character of the exchange interactions in the spin system (Néel 1948; Lowrie 1990; Tauxe 2014).

DISCUSSION

Demantoid is found in two types of geological settings: contact metamorphic skarn-type (e.g. Madagascar, Mexico, Namibia and Takab in Iran) and serpentinite-type (e.g. China, Italy, Pakistan, Russia, Slovakia and Kerman in Iran). Demantoid that forms in skarn-type deposits is usually associated with topazolite (±melanite) varieties of andradite, while serpentinite-hosted demantoid does not show this assemblage (Kievlenko 2003). This is also the case for Kerman demantoid, which formed in serpentinite. The distinct Cr^{3+} bands in the optical spectra confirm a serpentinite-related genesis for these samples. In general, the increase in absorption from 500 to 450 nm can be assigned to Fe^{2+}–O–Ti^{4+} charge transfer (e.g. Yu *et al*. 2019). As seen from the compositions listed in Tables II and III, there is no significant concentration of another transition metal that could be responsible for this band, other than traces of Mn (typically 410 nm for Mn^{2+}).

In the FTIR spectra, the OH^- mode energy (i.e. between 3660 and 3550 cm^{-1}) may be a function of the X- and Y-cation masses due to mode coupling and/or mixing. These OH^- modes have been assigned to a hydrogarnet substitution in the andradite end member, which has the same space as katoite (hydrogrossular), and four H^+ cations can substitute for Si without charge imbalance (Geiger & Rossman 2018). This is consistent with the appreciable water content of the serpentinite that hosts Kerman demantoid.

Serpentinite-hosted demantoid displays characteristic fibrous and acicular inclusions that are mostly chrysotile. These inclusions, which are a notable feature for the identification of demantoid, are typical in demantoid from Russia's Ural Mountains. In the literature, horsetails in demantoid from the Ural Mountains have been attributed to: (1) chrysotile asbestos (Alexandrov 1975; Kropantsev 1997); (2) byssolite (actinolite asbestos; Kropantsev 1997); and (3) tubular hollow channels, sometimes containing inclusions of chrysotile

[3] The Néel temperature describes a temperature limit at which an antiferromagnetic substance becomes paramagnetic.

or byssolite, or filled with other minerals such as limonite or serpentine (Kissin & Murzin 1990, 2015; Kissin *et al.* 2021). The presence of chrysotile fibres in demantoid from Kerman Province implies that the ultramafic host rocks (mainly serpentinised lherzolite) underwent hydrothermal alteration at temperatures no higher than about 400°C (Evans 2004), followed by decompression and autometasomatism. Serpentinisation and following autometamorphism made thermodynamically suitable conditions for the simultaneous sectoral growth of demantoid and formation of fibrous chrysotile inclusions (Holm *et al.* 2015).

Using Raman spectroscopy, it is possible to identify—to a certain extent—garnet end members or intermediate compositions. Kolesov and Geiger (1998) indicated that garnets have three main Raman bands that are sensitive to their composition, which can be used as a tool to calculate their approximate chemical composition and to estimate if they are (near) end members or have an intermediate solid-solution composition. These bands are found at about 350, 550 and 900 cm^{-1}, and are related to Si-O stretching, Si-O bending and $R(SiO_4)^{4-}$ rotational vibrations, respectively. The main characteristic Raman peaks for the studied demantoid samples are at about 353, 371, 515, 817, 841 and 875 cm^{-1} (see Figure 11). These are slightly different from the peaks reported for andradite by Kolesov and Geiger (1998), which could imply a solid-solution composition between andradite and uvarovite. These fingerprint characteristics of the Raman spectra obtained for our Kerman samples are identical to those of their Russian counterparts and, therefore, cannot be used for separating demantoid from these two localities. The EDXRF and GemTOF results also show that Kerman demantoid is predominantly of the andradite-uvarovite solid-solution series with 85–98% molar proportion of andradite (Figure 13).

The concentrations of some trace elements (e.g. Cr, Ge, Ni and Co) are significantly high in Kerman demantoid. The relatively high content of Cr in our samples, which is responsible for their typically deep green hue, is consistent with the results of Bocchio *et al.* (2010). There is a strong positive correlation between Ca and Cr (Figure 14a). This is consistent with lherzolitic[4] garnet (coexisting with clinopyroxene), and confirms lherzolite rather than harzburgite as the primary host rock (prior to serpentinisation) for Kerman demantoid. By contrast, a harzburgitic trend of garnet composition features a weaker correlation between Ca and Cr (Hill *et al.* 2015). A strong negative correlation between Fe and Cr is consistent with a major bulk-composition control on Fe content in the original ultramafic host rocks through melt removal in the shallower parts of the lithospheric mantle (Griffin *et al.* 1999).

A plot of Cr_2O_3 vs MnO/TiO_2 appears useful for separating Iranian demantoid from other localities (Figure 14b). Our Iranian samples show a Mn/Ti ratio greater than 1, while the available data for Russian and Pakistani demantoid yields a ratio between 0.1 and 1. In addition, relatively lower Cr concentrations are found in demantoid from Russia (Murzin *et al.* 1995; Bocchio *et al.* 2010; Pei *et al.* 2019) and Pakistan (Bocchio *et al.* 2010; Adamo *et al.* 2015) as compared to Iranian material. In demantoid from Namibia and Madagascar the Cr concentration is very low (Cairncross & Bahmann 2006; Pezzotta *et al.* 2011).

Although the concentrations of Ga and Ge are rather low in silicate-rich parts of the earth (i.e. crust and upper mantle), these elements can substitute for Al and Si in silicates at high pressure. This is because the ratio of the ionic radius of O to Si at high pressure is similar to that of O to Ge at low pressure (White 2013). The presence of Ge in the studied demantoid samples therefore implies that they formed under high-pressure conditions. U and Th have very low concentrations in the mantle where the ultramafic-related host rocks originally formed. The presence of rare-earth elements (REE) in demantoid is

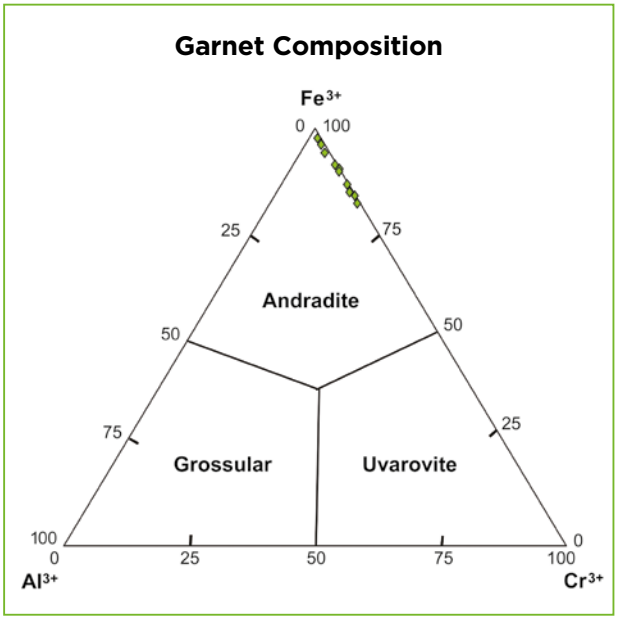

Figure 13: This ternary classification diagram for ugrandite garnets shows that Kerman demantoid compositions plot in the andradite field and contain varying amounts of the uvarovite component (Cr).

[4] Lherzolite is a type of peridotite containing olivine, orthopyroxene and clinopyroxene that formed in the earth's mantle.

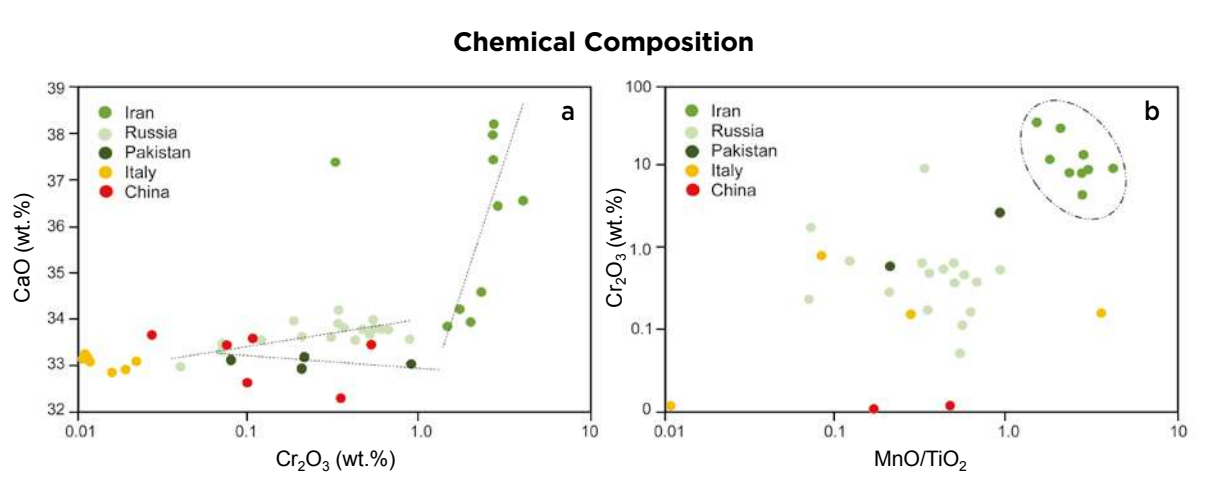

Figure 14: (**a**) This plot of CaO vs Cr_2O_3 (with the latter shown on a logarithmic scale) can help separate demantoid from Iran (this study), Russia (data from Murzin *et al.* 1995; Pei *et al.* 2019), Pakistan (Adamo *et al.* 2015), Italy (Adamo *et al.* 2009) and China (Liu *et al.* 1986), which all come from serpentinite host rocks. Note that the correlation trend of Ca vs Cr in Iranian demantoid is highly positive, while Russian demantoid exhibits a slightly positive correlation trend, and the available data from Pakistani and Chinese demantoids show a slightly negative correlation trend. Data for Italian garnets does not show a meaningful trend. (**b**) A logarithmic plot of Cr_2O_3 vs MnO/TiO_2 also provides a way to separate Iranian demantoid from the other localities. Further, it illustrates how Iranian demantoid typically contains a significantly higher Cr content than in stones from the other localities.

not unusual (e.g. Ayres & Harris 1997; Klimpel *et al.* 2021). Both heavy rare-earth elements (HREE) and light rare-earth elements (LREE) have relatively low concentrations in our samples (see Table III), but HREEs are enriched (relative to chondrite standard) in some samples. The REE concentrations in Kerman demantoid—with an average total of 1.76 ppmw (Table III)—are significantly lower than in stones of Russian origin, which average 4.85 ppmw (Pei *et al.* 2019). The overall abundance of LREE compared to HREE is similar in demantoid from both Iran and Russia.

Magnetic susceptibility was found to be similar for all our Iranian demantoid samples, particularly nos. 3–9 (Figure 15). This could be expected because the total amount of Fe + Cr (the elements with the strongest paramagnetic susceptibility) was similar in our specimens. The susceptibility is isotropic, which would be expected for a mineral of the cubic crystal system in which

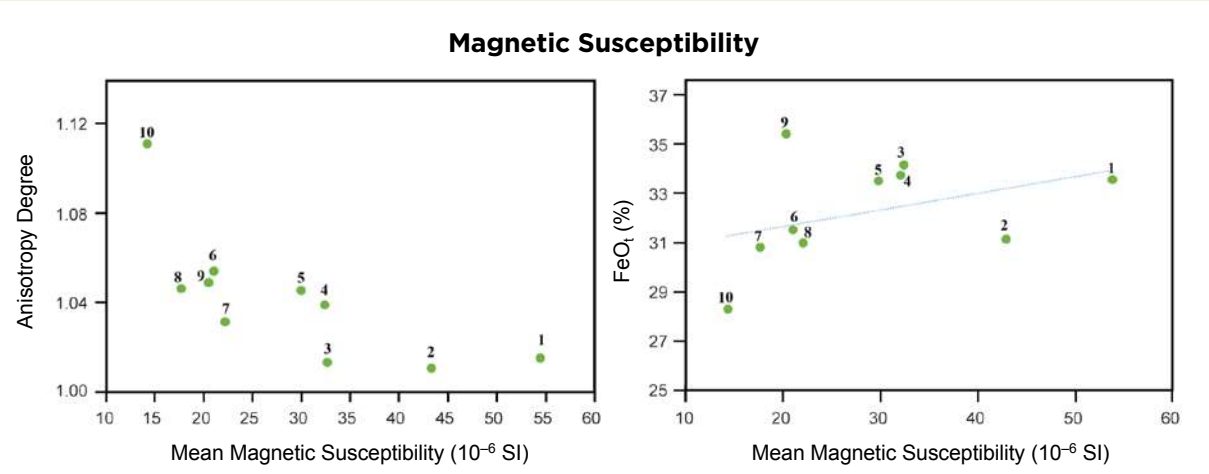

Figure 15: (**a**) The relationship between mean magnetic susceptibility and anisotropy degree for Kerman demantoid is similar for all samples, especially nos. 3–9. (**b**) The mean magnetic susceptibility shows a weak positive correlation with increasing Fe concentration. This suggests that the bulk magnetic susceptibility is mainly related to the Fe content of these garnets.

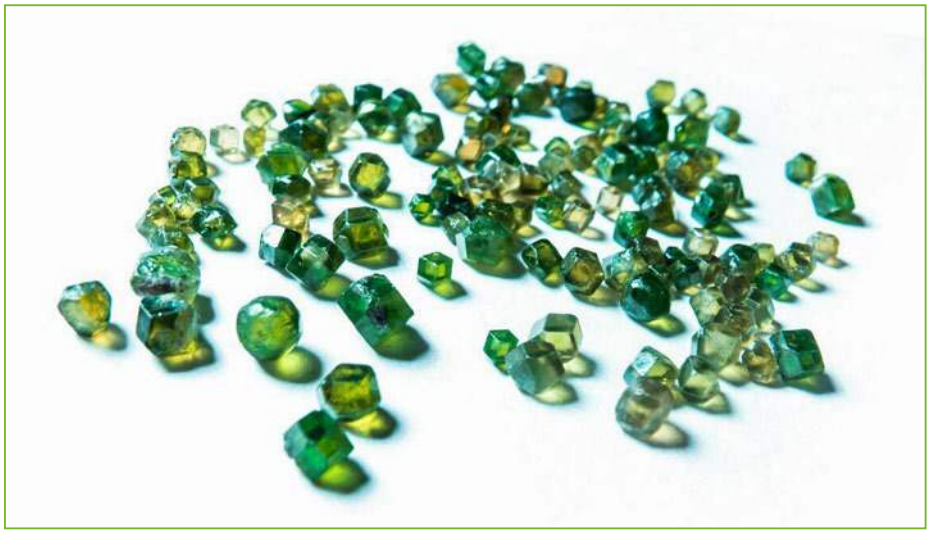

Figure 16: These crystals of demantoid (and topazolite) from Kerman Province weigh up to about 1 g and show good transparency. Photo by A. Badamegan.

Fe and Cr are distributed homogeneously within the lattice structure. A study by Frost (1960) of the magnetic susceptibility of garnets showing various compositions demonstrated that the susceptibility in the pyrope-almandine solid-solution series is linearly related to Fe content (Bleil & Petersen 1982). The higher the Fe content, the greater the susceptibility. Frost (1960) analysed one andradite sample and found a value of 6.31×10^{-7} m^3/kg, which is in good agreement with the results of our study. We also have shown that Kerman demantoid remains paramagnetic to at least 30 K, and would undergo antiferromagnetic ordering at very low temperature with an asymptotic Néel temperature of approximately –41.9 K.

CONCLUSIONS

Demantoid from Kerman Province in south-eastern Iran forms transparent to semi-transparent crystals with yellowish green to vivid or deep green colour. Crystals are occasionally very large (up to several dozen grams), but most are much smaller (e.g. Figure 16), so faceted stones tend to be small. The optical absorption spectra and chemical data obtained in this study are consistent with demantoid from serpentinite host rocks. Both Cr and Fe contribute significantly to the colour of Kerman demantoid. Raman spectroscopy revealed that the acicular inclusions in our samples consisted of chrysotile or open channels. Relatively high contents of trace elements such as Co, Ni, Ge and Cr are typical of Kerman demantoid, with low REE concentrations. Magnetic susceptibility measurements show that Kerman demantoid is paramagnetic.

Iran is an important source of gem-quality demantoid, while production from deposits in Russia has been decreasing in recent years. Demantoid is mainly found as rough material in the Iranian market, although some fine cut gemstones are also seen there. Jewellery containing demantoid is very rare in Iran, which is probably why this gem variety is not well known domestically. Fortunately, demantoid reserves in the Bagh Borj area of Kerman Province contain sufficient quantities to meet global market demand for decades.

REFERENCES

Adamo, I., Bocchio, R., Diella, V., Pavese, A., Vignola, P., Prosperi, L. & Palanza, V. 2009. Demantoid from Val Malenco, Italy: Review and update. *Gems & Gemology*, **45**(4), 280–287, https://doi.org/10.5741/gems.45.4.280.

Adamo, I., Gatta, G.D., Rotiroti, N., Diella, V. & Pavese, A. 2011. Green andradite stones: Gemmological and mineralogical characterisation. *European Journal of Mineralogy*, **23**(1), 91–100, https://doi.org/10.1127/0935-1221/2011/0023-2079.

Adamo, I., Bocchio, R., Diella, V., Caucia, F. & Schmetzer, K. 2015. Demantoid from Balochistan, Pakistan: Gemmological and mineralogical characterization. *Journal of Gemmology*, **34**(5), 428–433, https://doi.org/10.15506/JoG.2015.34.5.428.

Ahmadipour, H., Sabzehei, M., Whitechurch, H., Rastad, E. & Emami, M.H. 2003. Soghan complex as an evidence for paleospreading center and mantle diapirism in Sanandaj-Sirjan zone (south-east Iran). *Journal of Sciences, Islamic Republic of Iran*, **14**(2),

157–172, https://jsciences.ut.ac.ir/article_31685_02d519463548da0b9dc93843527737aa.pdf.

Alexandrov, A.I. 1975. Demantoid, chrome-containing andradite from Elizavetinskaya Bobrovska (Middle Urals). *Mineralogy and Petrography of the Urals, Sverdlovsk Institute of Mining*, **106**, 140–145.

Allen, M.B. & Armstrong, H.A. 2008. Arabia–Eurasia collision and the forcing of mid-Cenozoic global cooling. *Palaeogeography, Palaeoclimatology, Palaeoecology*, **265**(1–2), 52–58, https://doi.org/10.1016/j.palaeo.2008.04.021.

Amthauer, G. & Rossman, G.R. 1998. The hydrous component in andradite garnet. *American Mineralogist*, **83**(7–8), 835–840, https://doi.org/10.2138/am-1998-7-815.

Ayres, M. & Harris, N. 1997. REE fractionation and Nd-isotope disequilibrium during crustal anatexis: Constraints from Himalayan leucogranites. *Chemical Geology*, **139**(1–4), 249–269, https://doi.org/10.1016/s0009-2541(97)00038-7.

Barrois, O., Giuliani, G., Hafeznia, Y., Zeenabad, H.A., Rakotondrazafy, A.F.M., Ohnenstetter, D., Fallick, A.E., Mathieu, S. *et al*. 2012. Caractéristiques minéralogique et chimique des demantoides de Bagh Borj (Iran) et d'Antetezambato (Madagascar) : Consequences géologiques, 1ère partie, cadre géologique. *Revue de Gemmologie A.F.G.*, No. 182, 15–19.

Barrois, O., Giuliani, G., Hafeznia, Y., Zeenabad, H.A., Rakotondrazafy, A.F.M., Ohnenstetter, D., Fallick, A.E., Mathieu, S. *et al*. 2013. Caractéristiques minéralogique et chimique des demantoides de Bagh Borj (Iran) et d'Antetezambato (Madagascar) : Consequences géologiques, 2ème partie, études minéralogique et chimique. *Revue de Gemmologie A.F.G.*, No. 183, 10–15.

Biedermann, A.R., Pettke, T., Reusser, E. & Hirt, A.M. 2014. Anisotropy of magnetic susceptibility in natural olivine single crystals. *Geochemistry, Geophysics, Geosystems*, **15**(7), 3051–3065, https://doi.org/10.1002/2014GC005386.

Bleil, V. & Petersen, N. 1982. Magnetic properties of natural minerals: Paramagnetism. *In*: Angenheister, G. (ed) *Physical Properties of Rocks (Landolt-Börnstein: Numerical Data and Functional Relationships in Science and Technology–New Series–Group 5, Volume 1b)*. Springer-Verlag, Berlin, Germany, 312–320.

Bocchio, R., Adamo, I. & Diella, V. 2010. The profile of trace elements, including the REE, in gem-quality green andradite from classic localities. *Canadian Mineralogist*, **48**(5), 1205–1216, https://doi.org/10.3749/canmin.48.5.1205.

Cairncross, B. & Bahmann, U. 2006. Minerals from the Goboboseb Mountains: Brandberg region, Namibia. *Rocks & Minerals*, **81**(6), 442–457, https://doi.org/10.3200/rmin.81.6.442-457.

Celâl Şengör, A.M. 1984. *The Cimmeride Orogenic System and the Tectonics of Eurasia*. Geological Society of America Special Paper 195, 74 pp., https://doi.org/10.1130/SPE195-p1.

Douman, M. & Dirlam, D. 2004. Gem News International: Update on demantoid and cat's-eye demantoid from Iran. *Gems & Gemology*, **40**(1), 67–68.

Du Toit, G., Mayerson, W., van der Bogert, C., Douman, M., Befi, R., Koivula, J.I. & Kiefert, L. 2006. Demantoid from Iran. *Gems & Gemology*, **42**(3), 131.

Eichmann, E. 1870. Nils von Nordenskiöld. *Transactions of the St. Petersburg Emperor's Mineralogical Society, Series 2*, **5**, 189–192.

Emami, M.H., Mir Mohammad Sadeghi, M. & Omrani, S.J. 1993. *Magmatic map of Iran, 1:1,000,000*. Geological Survey of Iran, Tehran, Iran.

Evans, B.W. 2004. The serpentinite multisystem revisited: Chrysotile is metastable. *International Geology Review*, **46**(6), 479–506, https://doi.org/10.2747/0020-6814.46.6.479.

Feral, K. 2010. *Magnetic Susceptibility Index for Gemstones*, https://tinyurl.com/2c7wsnyc, accessed 25 October 2022.

Fergusson, C.L., Nutman, A.P., Mohajjel, M. & Bennett, V.C. 2016. The Sanandaj–Sirjan zone in the Neo-Tethyan suture, western Iran: Zircon U–Pb evidence of late Palaeozoic rifting of northern Gondwana and mid-Jurassic orogenesis. *Gondwana Research*, **40**, 43–57, https://doi.org/10.1016/j.gr.2016.08.006.

Frost, M.J. 1960. Magnetic susceptibility of garnet. *Mineralogical Magazine*, **32**(250), 573–576, https://doi.org/10.1180/minmag.1960.032.250.07.

Gaft, M., Reisfeld, R. & Panczer, G. 2005. *Modern Luminescence Spectroscopy of Minerals and Materials*. Springer-Verlag, Berlin, Germany, xvi + 356 pp., https://doi.org/10.1007/b137490.

Geiger, C.A. & Rossman, G.R. 2018. IR spectroscopy and OH^- in silicate garnet: The long quest to document the hydrogarnet substitution. *American Mineralogist*, **103**(3), 384–393, https://doi.org/10.2138/am-2018-6160CCBY.

Ghazi, J.M., Moazzen, M., Rahghoshay, M. & Moghadam, H.S. 2011. The geodynamic setting of the Nain ophiolites, central Iran: Evidence from chromian spinels in the chromitites and associated rocks. *Ofioliti*, **36**(1), 59–76.

Gill, J.O. 1978. Demantoid: The complete story. *Lapidary Journal*, **32**(7), 1542–1545.

Griffin, W.L., Fisher, N.I., Friedman, J., Ryan, C.G. & O'Reilly, S.Y. 1999. Cr-pyrope garnets in the lithospheric mantle. I. Compositional systematics and

relations to tectonic setting. *Journal of Petrology*, **40**(5), 679–704, https://doi.org/10.1093/petroj/40.5.679.

Hennebois, U., Delaunay, A., Karampelas, S. & Fritsch, E. 2021. *G&G* Micro-World: Faceted demantoid garnet with spectacular "horsetail" inclusions. *Gems & Gemology*, **57**(4), 384.

Hill, P.J.A., Kopylova, M., Russell, J.K. & Cookenboo, H. 2015. Mineralogical controls on garnet composition in the cratonic mantle. *Contributions to Mineralogy and Petrology*, **169**(2), article 13 (20 pp.), https://doi.org/10.1007/s00410-014-1102-7.

Holm, N.G., Oze, C., Mousis, O., Waite, J.H. & Guilbert-Lepoutre, A. 2015. Serpentinization and the formation of H_2 and CH_4 on celestial bodies (planets, moons, comets). *Astrobiology*, **15**(7), 587–600, https://doi.org/10.1089/ast.2014.1188.

Hoover, D.B. 2011. Determining garnet composition from magnetic susceptibility and other properties. *Gems & Gemology*, **47**(4), 272–285, https://doi.org/10.5741/gems.47.4.272.

Hoye, G.S. & O'Reilly, W. 1972. A magnetic study of the ferro-magnesian olivines $(Fe_xMg_{1-x})SiO_4$, $0 < x < 1$. *Journal of Physics and Chemistry of Solids*, **33**(7–9), 1827–1834, https://doi.org/10.1016/S0022-3697(72)80476-1.

Jasinevicius, R. 2009. *Characterization of vibrational and electronic features in the Raman spectra of gem minerals*. M.S. thesis, University of Arizona, Tucson, Arizona, USA, 151 pp., https://www.geo.arizona.edu/Antevs/Theses/JasineviciusThesis.pdf.

Karampelas, S., Gaillou, E., Fritsch, E. & Douman, M. 2007. Les grenats andradites-démantoïdes d'Iran : Zonage de couleur et inclusions. *Revue de Gemmologie A.F.G.*, No. 160, 14–20.

Kiefert, L. & Koivula, J.I. 2005. Idol's eyes: Chatoyant demantoid. *AGTA GTC's Laboratory Update*, May.

Kievlenko, E.Y. 2003. *Geology of Gems*. Ocean Pictures Ltd, Littleton, Colorado, USA, 432 pp.

Kissin, A.Y. & Murzin, V.V. 1990. New data on inclusions in the Urals demantoid. *In*: *Urals Summer Mineralogist School-97*, Ural State Academy of Mining and Geology, Ekaterinburg, Russia, 153–155 (in Russian).

Kissin, A.Y. & Murzin, V.V. 2015. Horsetail-like inclusions in Urals demantoid. *All-Russian Conference with International Participation, "Deposits of Stone-Colored and Non-Metallic New Materials of Various Geodynamics Settings"*, Ekaterinburg, Russia, 43–47 (in Russian).

Kissin, A.Y., Murzin, V.V. & Karaseva, E.S. 2021. "Horsetail" inclusions in the Ural demantoids: Growth formations. *Minerals*, **11**(8), article 825 (13 pp.), https://doi.org/10.3390/min11080825.

Klimpel, F., Bau, M. & Graupner, T. 2021. Potential of garnet sand as an unconventional resource of the critical high-technology metals scandium and rare earth elements. *Scientific Reports*, **11**(1), article 5306 (10 pp.), https://doi.org/10.1038/s41598-021-84614-x.

Kolesov, B.A. & Geiger, C.A. 1998. Raman spectra of silicate garnets. *Physics and Chemistry of Minerals*, **25**(2), 142–151, https://doi.org/10.1007/s002690050097.

Kropantsev, S. 1997. Novo-Karkodinsky deposit of demantoid. *In*: *Urals Summer Mineralogist School-97*, Ural State Academy of Mining and Geology, Ekaterinburg, Russia, 132–142 (in Russian).

Krzemnicki, M.S. 1999. Diopside needles as inclusions in demantoid garnet from Russia: A Raman microspectrometric study. *Gems & Gemology*, **35**(4), 192–195, https://doi.org/10.5741/gems.35.4.192.

Laurs, B.M. (ed) 2002. Gem News International: Demantoid garnet from Iran. *Gems & Gemology*, **38**(1), 96.

Lind, T., Henn, U. & Bank, H. 1998. New occurrence of demantoid in Namibia. *Australian Gemmologist*, **20**(2), 75–79.

Liu, S.I 2010. Demantoid garnet cat's eye from Iran and Russia. *Journal of the Gemmological Association of Hong Kong*, **31**, 74–78.

Liu, G., Kang, X. & Zhang, L. 1986. On the genesis of demantoid from Xinjiang, China. *Chinese Journal of Geochemistry*, **5**(4), 381–390, https://doi.org/10.1007/BF02866713.

Lowrie, W. 1990. Identification of ferromagnetic minerals in a rock by coercivity and unblocking temperature properties. *Geophysical Research Letters*, **17**(12), 159–162, https://doi.org/10.1029/GL017i002p00159.

McQuarrie, N. & van Hinsbergen, D.J.J. 2013. Retrodeforming the Arabia-Eurasia collision zone: Age of collision versus magnitude of continental subduction. *Geology*, **41**(3), 315–318, https://doi.org/10.1130/g33591.1.

Milisenda, C., Henn, U. & Henn, J. 2001. Demantoide aus Pakistan. *Gemmologie: Zeitschrift der Deutschen Gemmologischen Gesellschaft*, **50**(1), 51–56.

Misiorowski, E.B. & Hays, N.K. 1993. Jewels of the Edwardians. *Gems & Gemology*, **29**(3), 152–171, https://doi.org/10.5741/gems.29.3.152.

Murzin, V.V., Mamin, N.A., Kissin, A.Y. & Demchuk I.G. 1995. Demantoid garnet mineralization of the Verh-Neivinskii alpinotype ultramafic intrusion (Urals). *3rd Bi-annual Meeting "Intergems"*, 24 June–1 July, Turnov, Czech Republic, 38–41.

Néel, L. 1948. Propriétés magnétiques des ferrites ; Ferrimagnétisme et antiferromagnétisme. *Annales de Physique*, **12**(3), 137–198, https://doi.org/10.1051/anphys/194812030137.

O'Donoghue, M. (ed) 2006. *Gems*, 6th edn. Butterworth-Heinemann, Oxford, xxix + 873 pp.

Palke, A.C. & Pardieu, V. 2014. Gem News International: Demantoid from Baluchistan Province in Pakistan. *Gems & Gemology*, **50**(4), 302–303.

Pavese, A., Diella, V., Pischedda, V., Merli, M., Bocchio, R. & Mezouar, M. 2001. Pressure-volume-temperature equation of state of andradite and grossular, by high-pressure and -temperature powder diffraction. *Physics and Chemistry of Minerals*, **28**(4), 242–248, https://doi.org/10.1007/s002690000144.

Pei, J., Huang, W., Zhang, Q. & Zhai, S. 2019. Chemical constituents and spectra characterization of demantoid from Russia. *Spectroscopy and Spectral Analysis*, **39**(12), 3849–3854 (in Chinese).

Petriglieri, J.R., Salvioli-Mariani, E., Mantovani, L., Tribaudino, M., Lottici, P.P., Laporte-Magoni, C. & Bersani, D. 2015. Micro-Raman mapping of the polymorphs of serpentine. *Journal of Raman Spectroscopy*, **46**(10), 953–958, https://doi.org/10.1002/jrs.4695.

Pezzotta, F., Adamo, I. & Diella, V. 2011. Demantoid and topazolite from Antetezambato, northern Madagascar: Review and new data. *Gems & Gemology*, **47**(1), 2–14, https://doi.org/10.5741/gems.47.1.2.

Phillips, W.R. & Talantsev, A.S. 1996. Russian demantoid, czar of the garnet family. *Gems & Gemology*, **32**(2), 100–111, https://doi.org/10.5741/gems.32.2.100.

Phyo, M.M., Wang, H.A.O., Guillong, M., Berger, A., Franz, L., Balmer, W.A. & Krzemnicki, M.S. 2020. U–Pb dating of zircon and zirconolite inclusions in marble-hosted gem-quality ruby and spinel from Mogok, Myanmar. *Minerals*, **10**(2), article 195 (18 pp.), https://doi.org/10.3390/min10020195.

Quinn, E.P. & Laurs, B.M. 2005. Gem News International: Demantoid from northern Pakistan. *Gems & Gemology*, **41**(2), 176–177.

Ricou, L.-E. 1994. Tethys reconstructed: Plates, continental fragments and their boundaries since 260 Ma from Central America to south-eastern Asia. *Geodinamica Acta*, **7**(4), 169–218, https://doi.org/10.1080/09853111.1994.11105266.

Rinaudo, C., Gastaldi, D. & Belluso, E. 2003. Characterization of chrysotile, antigorite and lizardite by FT-Raman spectroscopy. *Canadian Mineralogist*, **41**(4), 883–890, https://doi.org/10.2113/gscanmin.41.4.883.

Shahraki-Ghadimi, A., Sahandi, M.R., Atapour, H., Poshtkuhi, M. & Zolfaghari, S. 2002. *1:100,000 Geological Map of Esfandaqeh (Geological Maps of Iran, Sheet 7447)*. Geological Survey of Iran, Tehran, Iran.

Sigamony, A. 1944. Magnetic susceptibility of diamond. *Proceedings of the Indian Academy of Sciences - Section A*, **19**(5), article 310 (5 pp,), https://doi.org/10.1007/bf03173459.

Stampfli, G.M. & Borel, G.D. 2002. A plate tectonic model for the Paleozoic and Mesozoic constrained by dynamic plate boundaries and restored synthetic oceanic isochrons. *Earth and Planetary Science Letters*, **196**(1–2), 17–33, https://doi.org/10.1016/s0012-821x(01)00588-x.

Tauxe, L. 2014. *Essentials of Paleomagnetism*. University of California Press, Berkeley, California, USA, 512 pp., https://doi.org/10.1525/9780520946378.

Wang, H.A.O. & Krzemnicki, M.S. 2021. Multi-element analysis of minerals using laser ablation inductively coupled plasma time of flight mass spectrometry and geochemical data visualization using t-distributed stochastic neighbor embedding: Case study on emeralds. *Journal of Analytical Atomic Spectrometry*, **36**(3), 518–527, https://doi.org/10.1039/d0ja00484g.

Wang, H.A.O., Krzemnicki, M.S., Chalain, J.-P., Lefèvre, P., Zhou, W. & Cartier, L. 2016. Simultaneous high sensitivity trace-element and isotopic analysis of gemstones using laser ablation inductively coupled plasma time-of-flight mass spectrometry. *Journal of Gemmology*, **35**(3), 212–223, https://doi.org/10.15506/JoG.2016.35.3.212.

White, W.M. 2013. *Geochemistry*. Wiley-Blackwell, Chichester, viii + 660 pp.

Yu, J., He, X. & Lu, Z. 2019. Cause analysis of chatoyancy of sapphires from Shandong, China. *RSC Advances*, **9**(42), 24420–24427, https://doi.org/10.1039/c9ra03585k.

The Authors

Dr Vahid Ahadnejad
Geology Department, Payame Noor University, 19395-4697 Tehran, Iran
Email: v.ahadnejad@pnu.ac.ir

Dr Michael S. Krzemnicki FGA
Swiss Gemmological Institute SSEF, Aeschengraben 26, CH-4051 Basel, Switzerland

Dr Ann Marie Hirt
Institute of Geophysics, ETH Zurich, Sonneggstrasse 5, CH-8092 Zurich, Switzerland

Acknowledgements

We are grateful to the Swiss Gemmological Institute SSEF and the Institute of Geophysics of ETH Zurich for their cooperation in the analysis of the samples. The assistance of Saeed Jabbari Bookani with the field trip of author VA is greatly appreciated.